

Character of eigenstates of the three- dimensional disordered Hamiltonian

J. Brndiar¹ and P. Markoš^{1,2}

¹*Institute of Physics, Slovak Academy of Sciences, 845 11 Bratislava, Slovakia*

²*Dept. Physics, Faculty of Electrical Engineering and Information Technology, Slovak University of Technology, Ilkovičova 3, 812 19 Bratislava, Slovakia*

We study numerically the character of electron eigenstates of the three dimensional disordered Anderson model. Analysis of the statistics of inverse participation ratio as well as numerical evaluation of the electron-hole correlation function confirm that there are no localized states below the mobility edge, as well as no metallic state in the tail of the conductive band. We discuss also finite size effects observed in the analysis of all the discussed quantities.

PACS numbers: 73.23.-b, 71.30., 72.10. -d

I. INTRODUCTION

Localization of electron in disordered systems,¹ manifests the wave character of the electron propagation. Components of the wave function, scattered on randomly distributed impurities, interfere with each other. This interference might lead to the electron localization.

While all states are localized in one dimensional systems, the localization of all electronic states in the three dimensional (3D) systems appears only when the strength of the disorder, W , exceeds certain critical value W_c . For weaker disorder, $W < W_c$, the energy band is divided into two parts, separated by the mobility edge E_c . It is supposed that all states with energy $|E| < E_c$ are metallic (conductive), while only localized states exist for $|E| > E_c$.

Although electron localization is easy to understand intuitively, the wave character of electron propagation causes new, nontrivial phenomena in all three transport regimes.

In the limit of weak disorder, the system is metal, but the scattering of electron on impurities is responsible for non-classical phenomena, such as the universal, system size independent conductance fluctuations^{2,3} and weak localization (antilocalization).^{4,5} The complete description of the transport was given by Green's function method,³ random matrix theory,^{2,6} DMPK equation⁷ or supersymmetric methods.⁸

In the opposite limit of strong disorder, (localized regime), the fluctuations of the conductance are so strong, (they exceed the mean conductance in many orders of magnitude), that the conductance itself is not a relevant parameter of the theory any more. Instead, the logarithm of the conductance must be studied.⁹

Owing to huge fluctuations, the analytical description of the critical regime is much more complicated. Thus, although the critical metal-insulator transition is well understood by the single parameter scaling,¹⁰ quantitative estimation of critical parameters is still almost unsolvable problem. Of particular interest is the critical exponent ν ¹¹ which determines the divergence of the correlation length, $\xi \propto |E - E_c|^{-\nu}$ at the mobility edge. Over two decades, there is a discrepancy between theoretical pre-

dictions and numerical estimations of ν . For 3D Anderson model, numerical results $\nu \approx 1.5 - 1.57$ obtained by various numerical methods^{12,13,14,15,16}, overestimate the analytical prediction, $\nu = 1$ ^{17,18}. The disagreement is even worse in 4D (numerical data^{19,20,21} give $\nu \approx 1$, while theory predicts $\nu = 0.5$). Numerical data for ν in low dimensional systems $d = 2 + \epsilon$ ($\epsilon \ll 1$)^{19,20} also do not agree with the analytical ϵ -expansions.¹¹

In our opinion, the origin of this discrepancy lies in the procedure of the averaging over the disorder.^{9,20} While averaging is extremely difficult to perform analytically it is straightforward in numerical simulations. Therefore, we expect that numerically obtained critical parameters will be, soon or later, supported by analytical results.^{22,23}

The inhomogeneous spatial distribution of electrons in the critical and localized regimes^{24,25} inspire people to build mean field theories on the the analysis of the statistics of the local density of state.^{26,27} Recent numerical data^{28,29} led to new analytical theories of the transport in the strongly localized regime.^{30,31,32}

In this paper we study numerically the character of eigenstates of the disordered 3D Anderson Hamiltonian. Our aim is to exclude any possibility for the existence of localized states below the mobility edge, E_c . The performed analysis is inspired by recent analytical theory of the Anderson transition³³ which predicts that the number of metallic states decreases continuously to zero when Fermi energy approaches the mobility edge from the metallic side. The idea is formulated in terms of the electron-hole correlation function $\Gamma_q(E, \omega)$ (defined later by Eqs. 3 and 4) which possesses in the limit of small energy difference ω and small wave vector q the diffusive pole of the form

$$\Gamma_q(E, \omega) = \frac{2\pi\rho(E)}{-iA(E)\omega + D(\omega)q^2}. \quad (1)$$

($\rho(E) = \text{Im } G(E + i\epsilon)/\pi$ is the density of states³⁴ determined by the one electron Green function $G(E + i\epsilon)$, and D is the diffusion constant).

Expression (1) differs from the “classical” diffusion pole¹⁷ by the presence of the function $A(E)$. It is claimed in Ref.³³ that $A(E)$ increases when E approaches the mobility edge and becomes infinite at the critical point. The

ratio $\rho(E)/A(E)$ determines the portion extended (diffusive) states from all available states, given by $\rho(E)$. The rest states, $\rho(E) \times (A - 1)/A$, are spatially localized, although E lies in the metallic phase, $|E| < E_c$.

Intuitively, the existence of localized states in the metallic phase seems to be impossible⁵. It also contradicts analytical analysis of the electron eigenstates^{8,35,36}. Nevertheless, no numerical analysis of this problem has been performed yet. The present paper fills this gap.

We investigate in Section II the singular behavior of $\Gamma_q(E, \omega) \sim \omega^{-1}$ for $q = 0$ and prove that $A(E) \equiv 1$ for all energies E , both in the metallic and localized regime. This confirms theoretical expectations^{17,25}. We also analyze the diffusive pole in the metallic phase (band center), find diffusive constant and discuss statistical properties of the function $\Gamma_q(E, \omega)$.

Another proof of the absence of localized states in the metallic phase is given in Section III, where we study the probability distribution of the inverse participation ratio (IPR)⁵ defined later by Eq. 11. Statistical properties of IPR were analytically studied in^{8,35,36}. Statistical properties of IPR at the critical point were subject of analytical and numerical analysis in connection to the multifractal spatial distribution of electrons.^{24,25,37} Scaling of IPR in the critical region was proved in³⁸. Here, we discuss how the probability distribution of IPR depends on the system size and the distance $E - E_c$ of the energy from the mobility edge. Our data show that the probability to find the localized state in the metallic phase decreases exponentially when the size of the system increases.

Electron eigenenergies and wave functions are calculated for the 3D Anderson Hamiltonian,

$$\mathcal{H} = \sum_{\vec{r}} \epsilon_{\vec{r}} c_{\vec{r}}^\dagger c_{\vec{r}} + V \sum_{[\vec{r}\vec{r}']} c_{\vec{r}}^\dagger c_{\vec{r}}. \quad (2)$$

Here, \vec{r} determines the site in the 3D lattice of the size L^3 , $\epsilon_{\vec{r}}$ is the random energy distributed with the Gaussian distribution, $P_G(\epsilon_{\vec{r}}) = (2\pi W^2)^{-1/2} \exp(-\epsilon_{\vec{r}}^2/2W^2)$. Parameter W measures the strength of the disorder and $V = 1$ determines the energy scale. For $E = 0$, the critical disorder $W_c \approx 6.15$. We fix the strength of the disorder $W = 2$ throughout this paper. Then, the mobility edge $E_c = 6.58$ separates the metallic and insulating phase.³⁸

II. THE ELECTRON-HOLE CORRELATION FUNCTION

In this section we investigate the electron-hole correlation function defined as

$$\Gamma(E, \omega, \vec{r}, \vec{r}') = \langle G(E + \omega/2 + i\epsilon, \vec{r}, \vec{r}') G(E - \omega/2 - i\epsilon, \vec{r}', \vec{r}) \rangle. \quad (3)$$

Here, $G(E + i\epsilon) = [E + i\epsilon - \mathcal{H}]^{-1}$ is the one-particle Green's function³⁴, which determines the density of states, and $\langle \dots \rangle$ means averaging over realization of the disorder.

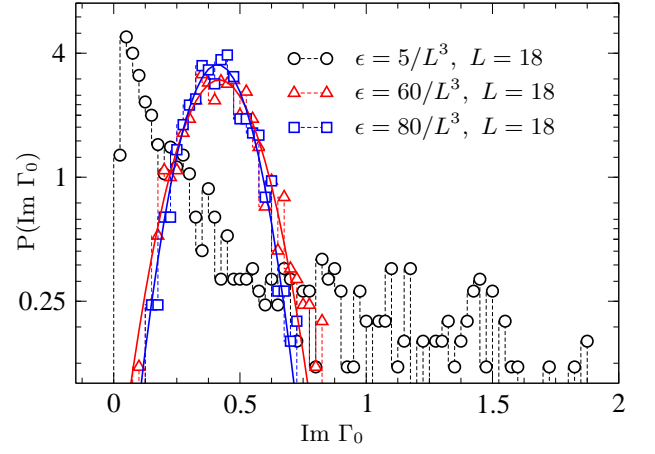


FIG. 1: (color online) Probability distribution $P(\text{Im } \Gamma_0)$ for $E = 7$, $\omega = 0.14$, $L = 18$ and for three values of ϵ . The density of states, $\rho(E = 7) \approx 0.0076$ and the mean level spacing is $\approx 130/L^3 \approx 0.0223$. The distribution obtained for $\epsilon = 5/L^3$ is clearly unphysical, but the choice $\epsilon = 60/L^3$ is already sufficient to reach the Gaussian distribution of $\text{Im } \Gamma_0$.

We calculate the Fourier transformation,

$$\Gamma_q(E, \omega) = \sum_{\vec{r}, \vec{r}'} e^{i\vec{q} \cdot (\vec{r} - \vec{r}')} \Gamma(E, \omega, \vec{r}, \vec{r}'), \quad (4)$$

set $q = 0$ and analyze the singular ω dependence

$$\Gamma_0(E, \omega) = \frac{B(E)}{-i\omega}, \quad \omega \rightarrow 0. \quad (5)$$

Comparison with Eq. (1) gives $B(E) = 2\pi\rho(E)$. Coefficient $B(E)$ would either equal to $2\pi\rho(E)$ (case $A \equiv 1$), or it would decrease to zero, $B(E) \sim (E_c - E)^\alpha$, if the scenario proposed in Ref.³³ is true.

Before presenting numerical data, it is worth to comment the numerical method of calculation of the Green's functions. Our method is based on the numerical inversion of the matrix $E \pm i\epsilon - \mathcal{H}$. For the reliability of data, the choice of the value of the small imaginary part of the energy, ϵ , is crucial. We expect that ϵ should be comparable to the typical level spacing, $1/(\rho(E)L^3)$. Using numerical data for the density of state at the band center, $\rho(E = 0) \approx 0.115$, we choose $\epsilon = 5/L^3$. This value is sufficiently large to avoid any numerical instabilities (discussed later in Sect. IIIC) in the band center, but it might be too small in the band tail, where the density of state is much smaller. Therefore, various larger values of ϵ were used to guarantee the numerical stability of our results.

As an example of how the value of ϵ influences the accuracy of numerical results, we show in Fig. 1 the probability distribution $P(\text{Im } \Gamma_0)$ for energy $E = 7$ and the system size $L = 18$. Statistical ensemble of $N = 2000$ samples was used to calculate the distribution. If ϵ is much smaller than the level spacing, then the distribution $P(\text{Im } \Gamma_0)$ consists of high peak close to zero, and very

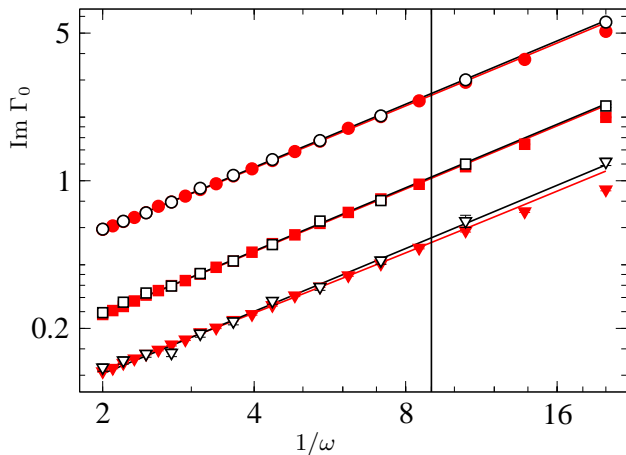


FIG. 2: (Color online) The imaginary part of $\Gamma_0(E, \omega)$, given by Eq. (5) as a function of ω^{-1} . $E = 5$, $L = 12$ (circles), $E = 6.58$, $L = 16$ (squares) and $E = 7$, $L = 18$ (triangles). $\epsilon = 5/L^3$ (open symbols). Higher values of ϵ were used to check the stability of data: $\epsilon = 15/L^3$ ($E = 6$), $40/L^3$ ($E = 6.58$) and $80/L^3$ ($E = 7$) (full symbols). Only data left of the vertical line were used for calculation of $B(E)$. Solid lines are fits $\ln \text{Im } \Gamma_0 = -\ln \omega + \ln B(E)$.

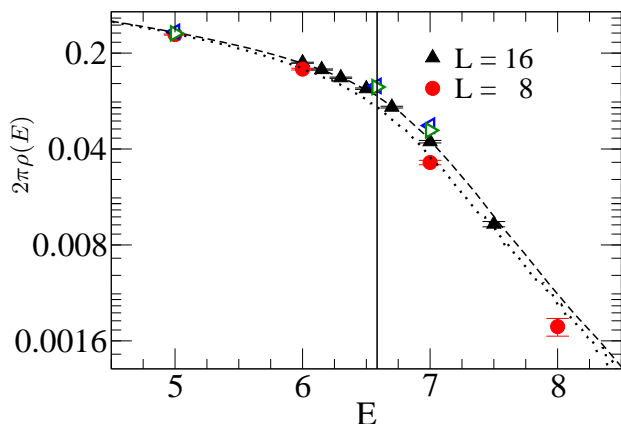


FIG. 3: (Color online) The coefficient $B(E)$ vs energy E compared with the density of states $2\pi\rho(E)$. Only critical region is shown. Deep in the metallic phase, the coincidence of $B(E)$ and $2\pi\rho(E)$ is even better. Size of the system is $L = 8$ (circles) and $L = 16$ (triangles). Open triangles show $B(E)$ calculated in Fig. 2 for $\epsilon = 5/L^3$ (triangle left) and for higher values of ϵ (triangle right). The density of states is calculated for $N_{\text{stat}} = 1000$ systems of the size $L = 16$ (dashed line) and $L = 8$ (dotted line). Dirichlet boundary conditions were used for calculation of both $\rho(E)$ and Γ_0 . Vertical line marks the position of the critical point.

long tail towards high values. This is because the density of states

$$\rho(E) = \left\langle \sum_n \delta(E - E_n) \right\rangle \approx \sum_n \frac{\epsilon/2\pi}{(E - E_n)^2 + \epsilon^2} \quad (6)$$

consists of set of very narrow separated peaks centered around eigenenergies E_n for small ϵ . Numerical data for

Γ_0 become reliable only for larger values of ϵ , for which the density of states is a smooth function of the energy. As shown in Fig. 1, P converges to the Gaussian distribution, independent on ϵ for sufficiently large values of ϵ .

A. Singularity of Γ_0 for $\omega \rightarrow 0$

Figure 2 shows numerical data for the imaginary part of $\Gamma_0(E, \omega)$ as a function of ω for three values of the energy $E = 5$, $E = 6.58$ (the mobility edge) and $E = 7$. Data prove the singular behavior $\Gamma_0 \sim 1/\omega$. Comparison of numerical data calculated for two and more different values of ϵ enable us also to estimate the accuracy of our results. Although the singularity $\sim 1/\omega$ transforms to $\text{Im } \Gamma_0 \sim \omega/(\omega^2 + \epsilon^2)$ when $\epsilon \neq 0$. $\text{Im } \Gamma_0$ becomes independent on ϵ for $\omega \gg \epsilon$ (the region left from the vertical line in Fig. 2). Only these data were used for the calculation of the coefficient $B(E)$.

In Fig. 3 we plot numerical data for the coefficient $B(E)$ and compare them with $2\pi\rho(E)$. The density of state $\rho(E)$ was calculated by direct diagonalizing of the Hamiltonian for $L = 8$ and $L = 16$. To increase the number of eigenstates, statistical ensembles of $N = 10^3$ samples were used for each L . As shown in Fig. 3, the density of states in the band tail still depends on the system size. Clearly, $L = 8$ is not sufficient for the calculation of ρ . To check the convergence of the density of states, we calculated the density of states for the energy $E = 7$, also from the statistical ensemble of samples of the size $L = 40$. The eigenenergies were calculated by Lanczos algorithm.³⁸ A comparison of the obtained density of states for $L = 16$ and 40 [$\rho(E = 7) = 0.0076$ for $L = 16$, and $\rho(E = 7) = 0.0087$ for $L = 40$] indicates that the convergence of the density of states is very slow in the band tail.

As shown in Fig. 3, obtained coefficient $B(E)$ agrees very well with our data for the density of states,

$$B(E) = 2\pi\rho(E). \quad (7)$$

The agreement is even better when we compare ρ and $B(E)$ calculated for the same system size. Since the size corrections of both $B(E)$ and $\rho(E)$ are positive (both quantities increases when L increases), we conclude that our data for $B(E)$ showed in Fig. 3 definitely exclude the possibility that $B(E)$ decreases to zero when E approaches the mobility edge.

B. Γ_q for non-zero q

In this section we calculate the electron-hole correlation function Γ_q for non-zero values of q . We show that numerical data are consistent with theoretical prediction. From numerical data, we estimate the diffusion constant D .

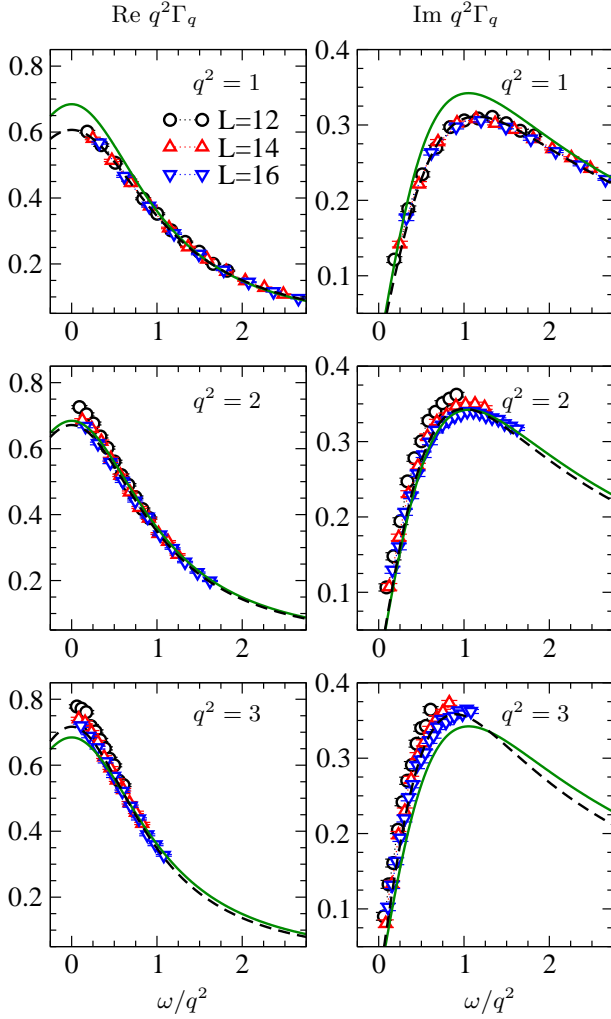


FIG. 4: The real and the imaginary part of $q^2\Gamma_q(E, \omega)$, given by Eq. (8), as a function of ω/q^2 for $E = 0$ (the band center) and for three values of q , $\vec{q} = (2\pi/L)[1, 0, 0]$, $(2\pi/L)[1, 1, 0]$ and $(2\pi/L)[1, 1, 1]$. Solid lines show theoretical prediction, given by Eq. (8), with $D = 1.055$. Dashed lines are fits of numerical data for $L = 16$ with $0.94 < D < 1.15$.

In general, D is a function of both ω and q . Numerical analysis of $D(\omega, q)$ for critical disorder $W = W_c$ and energy $E = 0$ was performed in Ref.³⁹ Numerical simulations confirmed scaling behavior of the diffusive constant in the critical regime, predicted theoretically.⁴⁰ Since the critical region around the mobility edge $E = E_c$ is very narrow,³⁸ we restrict our analysis to the metallic regime, $W = 2 \ll W_c$ and $E = 0$. Here, we expect that D is constant, independent on the frequency and wave vector.

Fig. 4 shows the real and the imaginary parts of the function $q^2\Gamma_q$,

$$q^2\Gamma_q(E, \omega) = \frac{2\pi\rho(E)}{-i\omega/q^2 + D}, \quad (8)$$

as a function of ω/q^2 . The size of the system is $L = 12, 14$ and 16 with periodic boundary conditions. Three values of the wave vector were considered: \vec{q} : $(1, 0, 0)$, $(1, 1, 0)$

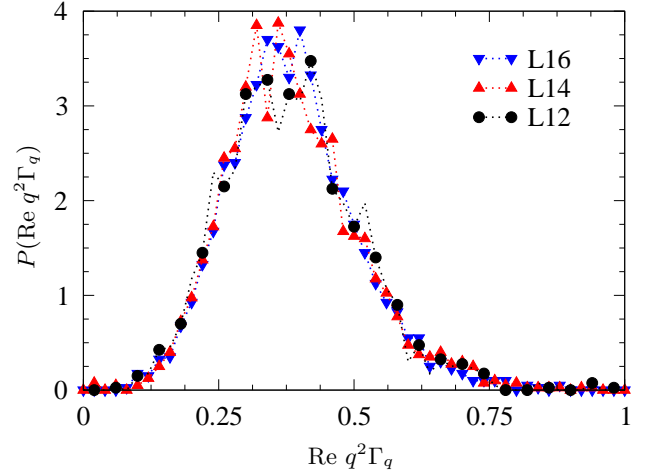


FIG. 5: (color online) The probability distribution of $q^2\Gamma_q$ for $q = 1$ and three system size, $L = 12, 14$ and 16 and $\omega/q^2 \approx 1$. The width of the distribution does not depend on the size of the system. The mean value, $\langle q^2\Gamma_q \rangle = 0.37$, and the variance, $\text{var } q^2\Gamma_q \approx 0.11$, does not depend on the size of the system.

and $(1, 1, 1)$ (in units of $2\pi/L$). As discussed above, $\epsilon = 5/L^3$ is already sufficient for numerical analysis of the electron-hole correlation function at the band center. We use this value in all calculations below.

Numerical data lie on the one universal curve. This universality is better pronounced for small values of q . Stronger finite size effects are observed for larger q . Data for $L = 16$ are fitted to Eq. (8) with fixed density of states, $2\pi\rho(E = 0) = 0.72$ and free parameter D . Fits are shown in Fig. 4 by dashed lines. From fits, we estimate the diffusion constant,

$$D \approx 1.05 \pm 0.10. \quad (9)$$

This value is compared with diffusion constant calculated by the transfer matrix method from the L -dependence of the conductance,

$$g(L) = \sigma L \quad (10)$$

where $\sigma = e^2 D(E) \rho(E)$ is the conductivity.²⁰ We obtained $D \approx 1.055$, which perfectly agrees with our estimation (9).

Finally, we present in Fig. 5 the probability distribution of real part of $q^2\Gamma_q$ for three sizes of the system $\omega/q^2 \approx 1$ for all systems. Our results confirm that the distribution depends only on the ratio ω/q^2 . This is consistent with Eq. (8). More important, data in Fig. 5 indicate that P does not depend on the system size.

III. INVERSE PARTICIPATION RATIO

The absence of localized states in the metallic phase can be demonstrated also by the analysis of the probability distribution of inverse participation ratio, defined

as^{5,25}

$$I(E_n) = \sum_r |\Phi_n(r)|^4. \quad (11)$$

Here, E_n and $\Phi_n(r)$ is the n th eigenenergy and eigenfunction of the Hamiltonian (2), respectively. If the $|E| < E_c$, then we expect that all eigenstates are conductive, with the wave functions distributed moreless homogeneously throughout the sample, so that $|\Phi_n(r)|^2 \propto L^{-d}$. Inserting in Eq. (11) we obtain that $I(E_n) \propto L^{-3}$ (in the 3D system). On the other hand, the wave function of localized electron is non-zero only in a small region, where $|\Phi_n(r)| \sim 1$. Hence, $I(E_n) \sim 1$. The size dependence of $I(E_n)$ in the critical region deserves more detailed analysis since the spatial distribution of electron is multifractal^{25,37} and $I \propto L^{-d_2}$ where $d_2 \approx 1.28$.³⁸

A. The size dependence of IPR

The energy spectrum of the Hamiltonian depends on the system size, L , and on the microscopic details of the disorder in a given sample. For a given system size, we consider a statistical ensemble of N_s samples which differ only in the realization of random energies, $\epsilon_{\vec{r}}$. For each sample, we calculate all eigenenergies, E_n , lying in a narrow energy interval, $E - \delta, E + \delta$, and calculate corresponding $I \equiv I(E_n)$. For the i th sample, the number of eigenstates, n_i , depends on the microscopic realization of the disorder.

Collecting $N_{\text{stat}} = \sum_i n_i$ values of IPR, we can construct its probability distribution $P(I)$ or $P(\ln I)$. Since the values of I might fluctuate in many orders in magnitude in the critical region⁸, it is more convenient to use

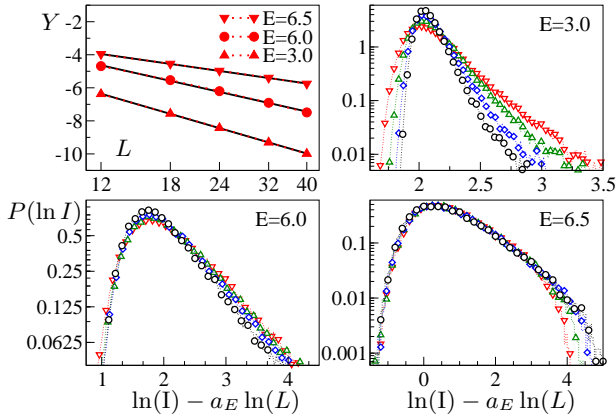


FIG. 6: (Color online) The left upper panel shows the system size dependence of $Y \propto a_E \ln L$ with $a_3 = -3.006$, $a_6 = -2.326$ and $a_{6.5} = -1.48$. Three other panels show the probability distribution $P(\ln I)$ for three energies of the electron and for the system size $L = 18$ (∇), 24 (\triangle), 32 (\diamond) and $L = 40$ (\circ). Note the scaling of the horizontal axis. $N_{\text{stat}} = 10^5$ eigenstates from the interval $|E_n - E| < 0.025$ were used for the statistics.³⁸

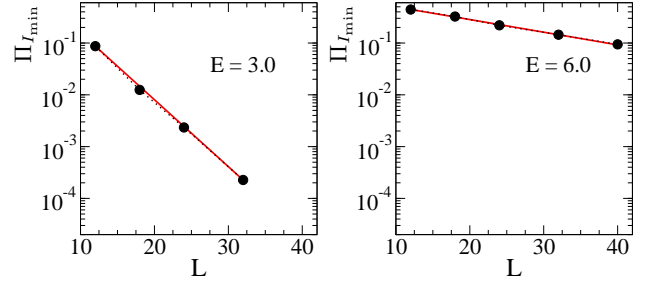


FIG. 7: (Color online) Left panel: The size dependence of the probability Π , defined by Eq. (14) with $I_{\min} = -2 \ln L$ for the energy $E = 3$. The right panel shows the probability $\Pi_{I_{\min}}$ for $I_{\min} = -3/2 \ln L$ and $E = 6$. Data confirm that $\Pi_{I_{\min}}$ decreases exponentially when the size of the system increases.

the logarithm of I and the mean value,

$$Y \equiv Y(E) = \frac{1}{N_{\text{stat}}} \sum_i \sum_{|E - E_n| < \delta} \ln I(E_n). \quad (12)$$

The upper left panel of Fig. 6 shows the system size dependence of Y for three energies below the mobility edge. We found that $Y \sim a_E \ln L$. In the metallic regime, we expect $a_E = -3$ for all $|E| < E_c$. At the mobility edge, $a_{E=E_c} = d_2$, the fractal dimension³⁸. For $E = 3$, which is the energy far below the mobility edge, we indeed find $a_3 = -3$, in agreement with our expectations. Higher values of a_E obtained for energies closer to the mobility edge are due to the finite size effects. We expect that a_E converges to -3 when the size of the system increases, $L \rightarrow \infty$. This is consistent with analytical expression for the mean IPR,³⁵

$$\langle I(L) \rangle = L^{-3} [1 + 4L/(\ell g)]. \quad (13)$$

Deep in the metallic regime, $|E| < E_c$, the conductance g is $\propto L$ (Eq. (10), so that Eq. (13) reproduces $\langle I \rangle \sim L^{-3}$. However, the linear increase of $g \sim L$ can be obtained only when the size of the system $L \gg \xi$. For smaller-size system, $L \sim \xi$, the correction term $4L/\ell g$ in Eq. (13) becomes L dependent and causes the deviation from the L^{-3} -dependence of mean I . The scaling behavior of IPR for energies close to the mobility edge is discussed later in section III C.

B. Probability distribution of IPR

Because of the randomness and wave character of the electron motion, the mean value of any quantity might not provide us with the entire information about the system. For instance, although $Y \propto -3 \ln L$, there still might exist some localized electronic states with an eigenvalue E_n and $\ln I \sim 0$. To measure the probability that insulating states exist in the metallic phase ($|E| < E_c$), we plot in Fig. 6 the probability distribution

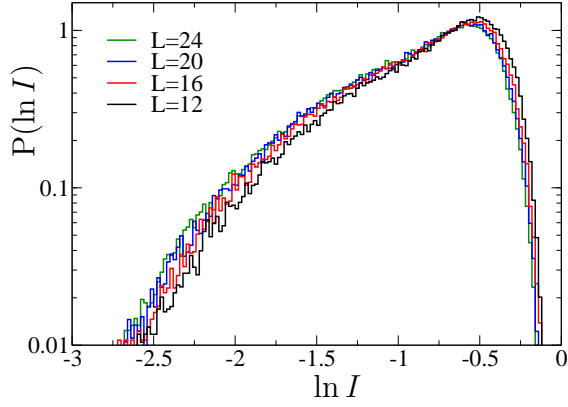


FIG. 8: (Color online) Probability distribution $P(\ln I)$ for the localized states for $L = 12, 16, 20$ and 24 . The distribution only weakly depends on the size of the system and decreases exponentially when $\ln I$ decreases. Consequently, the probability to find, for instance, the eigenstate with $\ln I < -\ln L$ decreases exponentially when L increases. Therefore, the probability to find the conductive state in the localized phase ($|E| > E_c$) is exponentially small.

$P(\ln I)$ calculated for three energies and various size of the system.

Data for $E = 3$ confirm that $P(\ln I)$ gets narrower when L increases. This is consistent with analytical result, $\text{var } I \sim L^{-2}$.³⁵ The narrowing of the probability distribution is less visible for energies close to the mobility edge E_c .

Since the mean value, Y , decreases as $\sim a_E \ln L$ when L increases, the existence of localized states is possible only if $P(\ln I)$ possesses a long tail which assures a non-zero probability to have $\ln I \sim 0$ for any system size. However, our data in Fig. 6 show that this is not the case. Contrary, $P(\ln I)$ decreases exponentially for $\ln I$ larger than Y . To measure this exponential decrease quantitatively, we calculate the probability that $\ln I$ is larger than certain value, I_{\min} :

$$\Pi_{I_{\min}} = \int_{I_{\min}}^{\infty} d \ln I' P(\ln I') = \int_{I_{\min}}^{\infty} dI' P(I') \quad (14)$$

We choose $I_{\min} = L^{-2}$ for $E = 3$ and $I_{\min} = L^{-3/2}$ for $E = 6.0$. In Fig. 7 we prove that $\Pi_{I_{\min}}$ decreases exponentially as a function of the size of the system L . This is consistent with theoretical prediction $P(I) \sim \exp(-\alpha I)$.⁸ Note, this exponential decrease is visible already for energies very close to the critical point, (right panel of Fig. 7). Since $I(E_n) \sim 1$ for the localized state E_n , the probability to observe the localized state inside the metallic phase decreases exponentially when the size of the system increases. We conclude that the probability to find any localized state is zero in the limit of $L \rightarrow \infty$.

Similar conclusion, namely that there are no metallic states in the energy interval $E > E_c$, can be derived for localized phase. In Fig. 8 we show the probability distribution $P(\ln I)$ for eigenstates around the energy

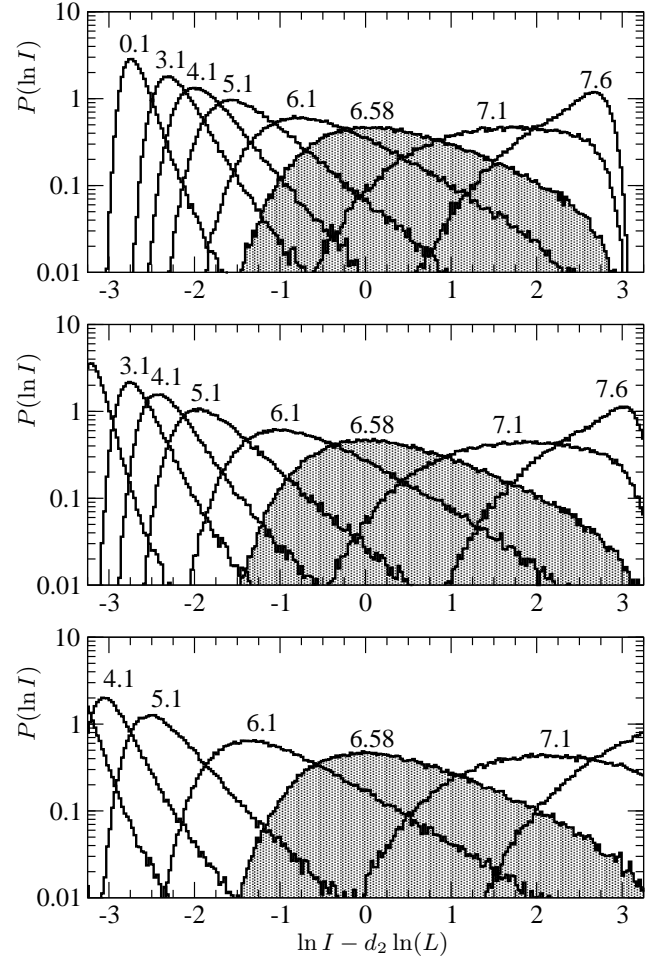


FIG. 9: Probability distribution $P(\ln I)$ for various energies, and three sizes of the system: $L = 12$ (top), $L = 16$ (middle) and $L = 24$ (bottom). Shaded area is the critical distribution P_c for $E = E_c$. Note, horizontal axis is scaled by $-d_2 \ln L$ in order to keep the critical distribution for $E_c = 6.58$ in the center of the figure.

$E = 7.5$. Clearly, the distribution is size independent, and decreases exponentially for small values of $\ln I$. Since metallic state requires that $\ln I \sim -3 \ln L$, we conclude that there are no metallic states in the insulating phase.

C. Finite size scaling

The right upper panel of Fig. 6 shows the distribution of IPR in the metallic regime. The distribution is centered at $3 \ln L$, in agreement with our expectation. More important is the form of the distribution for larger values of $\ln I$. Our data show that the probability to observe $\ln I \sim -2 \ln L$ decreases exponentially when the size of the system increases. Hence, we conclude that there are no localized states.

However, as is shown in lower panels of Fig. 6, narrowing of the distribution $P(\ln I)$ can be numerically ob-

served only when the energy E lies deep in the metallic phase. This is easy to understand. The metallic phase can be observed only in systems of size $L \gg \xi(E)$, where $\xi(E)$ is the correlation length.¹² Since $\xi(E)$ diverges as $\xi(E) \propto |E_c - E|^{-\nu}$ ($\nu \approx 1.57$ is the critical exponent) when $E \rightarrow E_c^-$, we cannot observe the metallic behavior for energies close to the mobility edge and for fixed size of the system. Nevertheless, reliable conclusion about the character of metallic states in the vicinity of the mobility edge can be drawn with the use of the finite size scaling analysis.¹⁰ The probability distribution $P(\ln I)$ depends both on the energy E and on the size of the system L . Following the scaling theory, P calculated for a given energy E and size L is equivalent to P obtained for E' closer to E_c , but larger system size $L' > L$.

Scaling of IPR in the critical region was numerically proved in Ref.³⁸. In Fig. 9 we demonstrate how the scaling idea works in the metallic phase. The distributions $P(\ln I)$ were calculated for various energies of the electron and for three size of the system. We see the similarity in the form of $P(\ln I)$ calculated for different E and L . For instance, the distribution for $E = 3.1$ and $L = 16$ is similar to the distribution for $E = 0.1$ and $L = 12$. Similarly, we can compare $E = 5.1$ and $L = 24$ with that for $E = 4.1$, $L = 12$. We also see that the form of the probability distribution $P(\ln I)$ only weakly depends on the energy E of the electron when $L \gg \xi(E)$. From this similarity we conclude that the properties of the distribution $P(\ln I)$ are universal in the metallic phase when $L \rightarrow \infty$. Therefore, the probability to find the localized state decreases to zero for any energy $|E| < E_c$.

IV. CONCLUSION

We studied numerically two parameters, important for the construction of the analytical theory of the metal-insulator transition. First, we verified the relation between electron-hole correlation function Γ and the density of states, Eq. (5). We proved that this relation not only holds for all energies of the electron, both in the

metallic and localized phase, but can be recovered for any size of the system. Our numerical procedure enables us to calculate, from Γ , the diffusion constant D . In the metallic limit, D agrees with estimation from the transfer matrix. Also, numerical data indicate that $\Gamma_q(E, \omega)$ is not the self-averaged quantity in the metallic regime.

It would be interesting to investigate also the scaling behavior of the diffusive constant in the critical regime.⁴⁰ Such analysis could confirm numerical scaling observed recently for the case of the critical disorder at band center.³⁹ However, since only frequencies $\omega > \epsilon$ are relevant in numerical data, we have to analyze much larger system size in order to fit both energies $E \pm \omega/2$ into the narrow critical region.³⁸

We also present numerical data for the mean values and for probability distributions of the inverse participation ratio. Our data, consistent with previous analytical results, enable us to prove that there are no localized states inside the metallic phase. All electron states are extended, and the probability to find the state which does not span through the sample decreases exponentially to zero when the size of the system increases. Similarly, no metallic states were observed on the opposite side of the critical point: in the insulating tail of the spectra, all electronic states are localized. Although this result seems to be easily accepted⁵, it was never proved numerically.

In contrast to the analytical theory, numerical methods do not enable the analysis of the behavior of any quantity in the limit of infinite system size. We can only describe how the variables of interest change when the size of the system increases. With the use of the finite size scaling hypothesis, we conclude that our results remain valid also in the limit of $L \rightarrow \infty$. Since all data were obtained without any additional assumption about the averaging procedure or the statistics of parameters of interest, they can serve as a starting point for the construction of the analytical theory of the Anderson transition.

This work was supported by grant APVV, project n. 51-003505 and VEGA, project n. 2/6069/26.

¹ P. W. Anderson, Phys. Rev. **109**, 1492 (1958).

² J. L. Pichard, in B. Kramer (Ed.) Quantum Coherence in Mesoscopic Systems, NATO ASI **254**, Plenum Press NY and London (1991).

³ P. A. Lee and A. D. Stone, Phys. Rev. Lett. **55**, 1622 (1985); P. A. Lee, A. D. Stone and H. Fukuyama, Phys. Rev. B **35**, 1039 (1987).

⁴ G. Bergmann, Phys. Rep. **107**, 1 (1984).

⁵ B. Kramer, A. MacKinnon, Rep. Progr. Phys. **56** 1469 (1993).

⁶ C. W. J. Beenakker, Rev. Mod. Phys. **69**, 731 (1997).

⁷ O. N. Dorokhov, JETP Lett. **36**, 318 (1982); P. A. Mello, P. Pereyra and N. Kumar, Ann. Phys. (N.Y.) **181**, 290 (1988).

⁸ A. D. Mirlin, Phys. Rep. **326**, 260 (2000).

⁹ P. W. Anderson, D. J. Thouless, E. Abrahams and D. S. Fisher, Phys. Rev. B **22i**, 3519 (1980)

¹⁰ E. Abrahams, P. W. Anderson, D. C. Licciardello, T. V. Ramakrishnan, Phys. Rev. Lett. **42**, 673 (1979).

¹¹ F. Wegner, Z. Phys. B **25**, 327 (1976); *ibid* **35**, 207 (1979); Nucl. Phys. B **316**, 623 (1989).

¹² A. MacKinnon, B. Kramer, Phys. Rev. Lett. **47** 1546 (1981); A. MacKinnon, B. Kramer, Z. Phys. B **53**, 1 (1983).

¹³ K. Slevin and T. Ohtsuki, Phys. Rev. Lett. **82**, 382 (1999)

¹⁴ K. Slevin, P. Markoš, T. Ohtsuki, Phys. Rev. Lett. **86**, 3594 (2001); Phys. Rev. B **67**, 155106 (2003).

¹⁵ B. I. Shklovskii, B. Shapiro, B. R. Sears, P. Lambrianides, H. B. Shore, Phys. Rev. B **47**, 11487 (1993)

¹⁶ I. Kh. Zharekeshev, B. Kramer, Phys. Rev. B **51**, 17239

- (1995)
- ¹⁷ D. Vollhardt, P. Wölfle, Phys. Rev. B **22**, 4666 (1980); D. Vollhardt, P. Wölfle: *Self-Consistent Theory of Anderson Localization*, in *Electronic Phase Transitions*, Ed. by W. Haake and Yu. V. Kopaeve, Elsevier Sci. Publ. (1992).
 - ¹⁸ I. M. Suslov, J. Exp. Theor. Phys. **101**, 661 (2005).
 - ¹⁹ I. Travněc and P. Markoš, Phys. Rev. B **65**, 113109 (2002)
 - ²⁰ P. Markoš, acta physica slovacica **56**, 561 (2006).
 - ²¹ A. M. Garcia-Garcia, E. Cuevas, Phys. Rev. B **75**, 174203 (2007)
 - ²² A. Kawabata, in T. Brandes and S. Kettelman (Editors) *Anderson Localization and its Ramifications*, Lecture Notes in Physics, Springer (2003)
 - ²³ A. Garcia-Garcia, arXiv:0709.1292
 - ²⁴ M. Janßen, Int. J. Mod. Phys. B **8**, 943 (1994).
 - ²⁵ F. Evers, A. D. Mirlin, arXiv:0707.4378
 - ²⁶ V. Dobrosavljevic, A. A. Pastor, B. K. Nikolic, Europhys. Lett. **62**, 76 (2003).
 - ²⁷ Yun Song, W. A. Atkinson, R. Wortis, Phys. Rev. B **76**, 045105 (2007)
 - ²⁸ P. Markoš, Phys. Rev. B **65**, 104207 (2002).
 - ²⁹ J. Prior, A. M. Somoza and M. Ortuno, Phys. Rev. B **72**, 024206; A. M. Somoza, J. Prior and M. Ortuno, Phys. Rev. B **73**, 184201 (2006).
 - ³⁰ K. A. Muttalib and J. R. Klauder, Phys. Rev. Lett. **82**, 4272 (1999); K. A. Muttalib and V. A. Gopar, Phys. Rev. B **66**, 115318 (2002).
 - ³¹ P. Markoš, K. A. Muttalib, P. Wölfle and J. R. Klauder, Europhys. Lett. **68**, 867 (2004); K. A. Muttalib, P. Markoš and P. Wölfle, Phys. Rev. B **72**, 125317 (2005); J. Brndiar, R. Derian and P. Markoš, Phys. Rev. B **76**, 155320 (2007).
 - ³² A. M. Somoza, M. Ortuno and J. Prior, Phys. Rev. Lett. **99**, 116602 (2007).
 - ³³ V. Janiš and J. Kolorenč, Phys. Rev. B **71**, 033103 (2005); V. Janiš and J. Kolorenč, Phys. Rev. B **71**, 245106 (2005); Phys. Stat. Sol. (B) **241**, 2032 (2004); Mod. Phys. Lett. B **18**, 1051 (2004).
 - ³⁴ E. N. Economou, *Green's Functions in Quantum Physics*, 2nd ed., Springer (1990).
 - ³⁵ Y. V. Fyodorov, A. D. Mirlin, Phys. Rev. B **51**, 13403 (1995)
 - ³⁶ V. I. Falko, K. B. Efetov, Phys. rev. B **52**, 17413 (1995).
 - ³⁷ F. Evers, A. D. Mirlin, Phys. Rev. Lett. **84**, 3690 (2000); A. D. Mirlin, F. Evers, Phys. Rev. B **62**, 7920 (2000); A. Mildenberger, F. Evers, A. D. Mirlin, Phys. Rev. B **66**, 033109 (2002). F. Evers, A. Mildenberger, A. D. Mirlin, Phys. Rev. B **64**, 241303(R) (2001); E. Cuevas, Phys. Rev. B **66**, 233103 (2002).
 - ³⁸ J. Brndiar, P. Markoš, Phys. Rev. B **74**, 153103 (2006); Lanczos algorithm based on <http://www.netlib.org/lanz/>.
 - ³⁹ T. Brandes, B. Huckestein and L. Schweitzer, Ann. Phys. **5**, 633 (1996).
 - ⁴⁰ J. T. Chalker, G. J. Daniell, Phys. Rev. Lett. **61**, 593 (1988); J. T. Chalker, Physica A **167**, 253 (1990).